THE JOURNAL OF BIOLOGICAL CHEMISTRY VOL. 284, NO. 50, pp. 34580–34589, December 11, 2009

The XcpV/GspI Pseudopilin Has a Central Role in the Assembly of a Quaternary Complex within the T2SS Pseudopilus*[S]

Received for publication, July 8, 2009, and in revised form, October 8, 2009 Published, JBC Papers in Press, October 14, 2009, DOI 10.1074/jbc.M109.042366

Badreddine Douzi[‡§], Eric Durand[¶], Cédric Bernard[‡], Sébastien Alphonse[‡], Christian Cambillau[‡], Alain Filloux[¶‖], Mariella Tegoni[‡], and Romé Voulhoux[¶1]

From the [‡]Architecture et Fonction des Macromolecules Biologiques, UMR6098, CNRS, and Universites d'Aix-Marseille I and II, 13288 Marseille Cedex 9, France, the [§]Laboratoire des Maladies Transmissibles et Substances Biologiquement Actives (LR99ES27), Faculté de Pharmacie, TU-5000 Monastir, Tunisia, the [¶]Laboratoire d'Ingénierie des Systèmes Macromoléculaires, UPR 9027, CNRS, Université de la Méditerranée, Institut de Microbiologie de la Méditerranée, 13402 Marseille Cedex 20, France, and the [‖]Centre for Molecular Microbiology and Infection, Division of Cell and Molecular Biology, Imperial College, London SW7 2AZ, United Kingdom

Gram-negative bacteria use the sophisticated type II secretion system (T2SS) to secrete a large number of exoproteins into the extracellular environment. Five proteins of the T2SS, the pseudopilins GspG-H-I-J-K, are proposed to assemble into a pseudopilus involved in the extrusion of the substrate through the outer membrane channel. Recent structural data have suggested that the three pseudopilins GspI-J-K are organized in a trimeric complex located at the tip of the GspG-containing pseudopilus. In the present work we combined two biochemical techniques to investigate the protein-protein interaction network between the five *Pseudomonas aeruginosa* Xcp pseudopilins. The soluble domains of XcpT-U-V-W-X (respectively homologous to GspG-H-I-J-K) were purified, and the interactions were tested by surface plasmon resonance and affinity co-purification in all possible combinations. We found an $XcpV_I$-W_J-X_K complex, which demonstrates that the crystallized trimeric complex also exists in the *P. aeruginosa* T2SS. Interestingly, our systematic approach revealed an additional and yet uncharacterized interaction between $XcpU_H$ and $XcpW_J$. This observation suggested the existence of a quaternary, rather than ternary, complex ($XcpU_H$-V_I-W_J-X_K) at the tip of the pseudopilus. The assembly of this quaternary complex was further demonstrated by co-purification using affinity chromatography. Moreover, by testing various combinations of pseudopilins by surface plasmon resonance and affinity chromatography, we were able to dissect the different possible successive steps occurring during the formation of the quaternary complex. We propose a model in which $XcpV_I$ is the nucleator that first binds $XcpX_K$ and $XcpW_J$ at different sites. Then the ternary complex recruits $XcpU_H$ through a direct interaction with $XcpW_J$.

The extracellular secretion of proteins by Gram-negative bacteria requires specialized secretion machineries to allow the selective passage through the normally impermeable envelope constituted by the cytoplasmic or inner membrane, the periplasm and the outer membrane (OM).[2] In type II secretion systems (T2SSs), exoproteins precursors are first translocated across the inner membrane via either the general export pathway (Sec) or the twin arginine translocation pathway (Tat) and then taken in charge by the secreton for OM translocation (1, 2). The secreton is a multiprotein complex involving at least 12 different proteins called $XcpA_O$, $XcpP_C$–Z_M[3] in our model organism, the Gram-negative bacterium, *Pseudomonas aeruginosa* (for review see Ref. 3). In the current model for the assembly of the Xcp secreton, three subcomplexes are defined: the inner membrane platform ($XcpR_ES_FY_LZ_M$), required for providing energy to the secretion process; the OM secretin $XcpQ_D$, forming a pore in the OM through which the substrate is secreted; and a third subcomplex called the pseudopilus by homology with the type IV pilus (T4P). Type 4 pili are long fimbrial structures present at the cell surface of various Gram-negative bacteria (4, 5). They are formed in the periplasm by the polymerization of the major pilin subunit. In *P. aeruginosa*, five Xcp proteins ($XcpT_G$ to $XcpX_K$) are, like type IV pilins, processed by the specific prepilin peptidase $XcpA_O$/PilD (6, 7) and have therefore been named pseudopilins. $XcpT_G$ is the most abundant and was therefore called the major pseudopilin (8), in contrast to $XcpU_H$, V_I, W_J, and X_K, which were named minor pseudopilins. $XcpA_O$/PilD cleaves a short leader peptide located at the extreme N terminus of the pilin/pseudopilin and preceding a highly conserved hydrophobic domain. This domain is followed by a less conserved C-terminal soluble domain.

In contrast to T4P, very little is known about the structural organization of the pseudopilus involved in type II secretion because such a structure could not be detected under physiological conditions. Recent works have shown that the major pseudopilin $XcpT_G$ is able, upon overproduction, to form an abnormally long pseudopilus also called hyperpseudopilus (HPP) protruding at the cell surface (9–11). This observation reveals that major pseudopilins such as $XcpT_G$ have the ability to pack into an helical complex similar to the type IV pilus.

* This work was supported by Agence Nationale de la Recherche Program "Jeune Chercheur" Grant ANR-JC07-183230 and by funds from the Royal Society (to A. F.).

[S] The on-line version of this article (available at http://www.jbc.org) contains supplemental Tables S1 and S2 and Figs. S1 and S2.

[1] To whom correspondence should be addressed: LISM-UPR 9027, CNRS, IMM, 31 Chemin Joseph Aiguier, 13402 Marseille cedex 20, France. Tel.: 33-4-91-16-41-26; Fax: 33-4-91-71-21-24; E-mail: voulhoux@ifr88.cnrs-mrs.fr.

[2] The abbreviations used are: OM, outer membrane; T2SS, type II secretion system; HPP, hyperpseudopilus; RM, reaction mixture; T4P, type 4 pilus.

[3] Because a different nomenclature is used for non-*Pseudomonas* T2SS, the alternative gene or protein nomenclature will also be indicated, for example in $XcpT_G$ the "G" will refer to GspG, which will reciprocally be called $GspG_T$.

According to this observation, the crystallographic structure of the major type II secretion pseudopilin $PulG_T$ shows an overall fold similar to the major type IV pilin monomer (12). It is a four-stranded anti-parallel β-sheet that forms a buried hydrophobic core with the N-terminal hydrophobic α-helix to create an $\alpha\beta$-roll (see Ref. 13 for review).

The structures of the four T2SS minor pseudopilins from *Escherichia coli* and various *Vibrio* species have recently been solved (14–17). Even though each pseudopilin displays specific motifs, they all show the typical $\alpha\beta$-fold, suggesting that they may physically be incorporated into the pseudopilus.

All of the pseudopilins are essential for secretion, but except for $XcpT_G$, none of them is able to form an HPP upon overproduction (18). Alternatively, specific functions have been considered for minor pseudopilins, such as a role for $XcpV_I$ in HPP initiation and for $XcpX_K$ in the control of HPP length (9, 18). Altogether these data suggest important accessory functions for the minor pseudopilins in the pseudopilus formation.

Several interactions between full-length pseudopilins have been previously detected by various biochemical and genetic approaches (8, 11, 18–21). Interestingly, interactions between the soluble domains were also detected, indicating that contacts between the pseudopilins are not restricted to the N-terminal hydrophobic domain which form the helical backbone as shown with the type IV pilus. The recent co-crystallization of *E. coli* $GspI_V$-J_W-K_X-soluble domains in a ternary complex confirms the capacity of these domains to directly interact (17).

In the present work we extended the study of the interaction network between the five pseudopilin-soluble domains using the *P. aeruginosa* Xcp T2SS as model system. By performing a combination of protein-protein interaction experiments, we brought more understanding into the sequential assembly of the four minor pseudopilins $XcpU_H$-V_I-W_J-X_K. We showed that these proteins could form a yet uncharacterized quaternary complex possibly present at the tip of the $XcpT_G$ pseudopilus. Moreover, our data converge toward the suggestion of a central role of $XcpV_I$ in the formation of the quaternary complex and subsequently for pseudopilus formation.

EXPERIMENTAL PROCEDURES

Nomenclature for Soluble Domains of Xcp Pseudopilins Produced and Used in This Study—All of the pseudopilin variants used in this study are deleted for their N-terminal hydrophobic domains; they are called pseudopilin-soluble domains. Then either histidine-tagged (^{his}N) or nontagged (N) soluble domains of pseudopilins were used in this study, where "N" designates any pseudopilins and "^{his}" designates the N-terminal six-histidine tag.

Cloning, Expression, and Purification of Untagged Soluble Domains of the Five Xcp Pseudopilins—The classical heterologous over-expression of the non-tagged minor pseudopilins V_I, U_H, W_J and X_K soluble domains did not give sufficient material. This technical problem was solved by fusing the four constructs to thioredoxin which gives to the construction a soluble character (22). In our constructs, thioredoxin is cleaved off after expression and the resulting proteins are soluble, stable and produced in sufficient amount for biochemical and biophysical characterization.

The DNA sequence encoding non-tagged soluble domain of $XcpT_G$ pseudopilin (T_G) (starting at the Methionine 25 relative to the prepiline peptidase cleavage site was cloned for a periplasmic expression into the Gateway pETG-22b expression vector (23) leading to plasmid pETG-22b-T_G (supplemental Table S1); a His_6 tag encoding DNA and the sequence encoding for a TEV protease cleavage site were inserted in frame between the attB1 and the sequence encoding T_G. Primers (T_G-Forward and T_G-Reverse) used for amplification are shown in supplemental Table S2.

The DNA sequence encoding nontagged soluble domains of XcpU, V, W, and X pseudopilins, respectively called V_I, U_H, W_J and X_K and corresponding to the residues serine 22 for V_I, serine 23 for U_H, arginine 22 for W_J, and arginine 23 for X_K relative to the prepiline peptidase cleavage site were cloned for cytoplasmic expression into the pETG-20A expression vector leading to plasmids pETG-20A-U_H, pETG-20A-V_I, pETG-20A-W_J, and pETG-20A-X_K (supplemental Table S1). The resulting constructions thus contain a N-terminal thioredoxin sequence, followed by a His_6 tag, the attB1, a His_6 tag, and the TEV protease cleavage site. The primers (U_H-V_I-W_J-X_K-Forward and -Reverse) used for amplification of soluble domains of following pseudopilins are presented in supplemental Table S2.

E. coli BL21 (DE3) pLys-S (Invitrogen) cells were transformed with pET-22b-T_G. Precultures grown on Luria Broth at 37 °C were used to start the culture (A_{600} = 0.4) at 37 °C in auto-inductor ZYP-5052 medium (BNL; rich medium containing yeast extract, tryptone, phosphate-buffer, 0.05% glucose, 0.5% glycerol, and 0.2% lactose). At A_{600} = 0.8, the temperature was decreased to 30 °C, and the cells were cultivated for 18 h. Ampicillin (100 μg/ml) and chloramphenicol (35 μg/ml) were present continuously during expression. The periplasmic purification of T_G, in line with the procedure described in Ref. 18, started with an osmotic shock followed by dialysis against 50 mM phosphate buffer, 150 mM NaCl, pH 8, overnight at 4 °C. The resulting fraction goes through the chromatographic steps as specified below for the other pseudopilins.

E. coli BL21 (DE3) pLys-S cells were transformed with pETG-20A-U_H, pETG-20A-V_I, pETG-20A-W_J, and pETG-20A-X_K. Precultures grown on Luria Broth at 37 °C were used to inoculate large cultures in ZYP-5052 auto-inductor medium. In the case of V_I, the culture was carried on at 30 °C for 24 h. In the case of U_H, W_J, and X_K, the cultures were carried on at 37 °C. At A_{600} = 0.8, the temperature was decreased at 17 °C, and the cells were allowed to grow for 24 h. The precultures and cultures were performed in presence of ampicillin (100 μg/ml) and chloramphenicol (35 μg/ml). The cytoplasmic purification of U_H, V_I, W_J, and X_K started by a cell lysis step was performed at 4 °C. The cells were resuspended in lysis buffer (50 mM Tris, pH 8.0, 300 mM NaCl, 1 mM EDTA, 0.5 μg/ml lysozyme, phenylmethylsulfonyl fluoride), submitted to three freeze-thawing cycles, and sonicated after the addition of DNase at 20 μg/ml and $MgCl_2$ at 20 mM. The pellet and soluble fraction were separated by centrifugation for 30 min at 16,099 × *g*.

Soluble fractions containing T_G-U_H-V_I-W_J-X_K were 1) dialyzed against 50 mM Tris, 150 mM NaCl, pH 8.0; 2) loaded on a nickel (HisTrap™ FF crude column 1.6 × 2.5 cm (5 ml)) on ÄKTA Express (Amersham Biosciences) pre-equilibrated in

50 mM Tris, 300 mM NaCl, 10 mM Imidazole, pH 8.0; 3) eluted by washing with 50 mM Tris, 300 mM NaCl, pH 8.0, in the presence of 250 mM imidazole; 4) desalted on HiPrep 26/10 Desalting column (Sephadex™ G-25; Amersham Biosciences); 5) cleaved by the TEV protease 1 mg/ml (4 °C, 18 h); and 6) loaded on a nickel column pre-equilibrated in 50 mM Tris, 300 mM NaCl, 10 mM imidazole, pH 8.0, which selectively retard both the TEV and the fusion protein, which are still His_6-tagged. The untagged pseudopilin was recuperated in the flow-through and concentrated on Centricon (cut-off 3 kDa). After concentration, the pseudopilins were passed through a Sephadex G75 equilibrated in 50 mM phosphate, 150 mM NaCl, pH 7.

The final concentrations of the proteins were calculated on the value of $A_{280\,nm}$ by using the following extinction co-efficients found by ProtParam (T_G 12,000 $(mg/ml)^{-1}$; V_I 11,563 $(mg/ml)^{-1}$; U_H 16,177 $(mg/ml)^{-1}$; W_J 24,169 $(mg/ml)^{-1}$; X_K 34,071 $(mg/ml)^{-1}$). The yields were 4, 8, 8, 18, and 11 mg/liter of T_G, V_I, U_H, W_J and X_K, respectively, evaluated by NanoDrop (Thermo Scientific).

Cloning and Expression of the His_6-tagged Soluble Domains of Xcp Pseudopilins—The DNA sequence encoding His_6-tagged soluble domains of $XcpT_G$, U_H, W_J, and X_K pseudopilins, respectively called $^{his}T_G$, $^{his}U_H$, $^{his}W_J$, and $^{his}X_K$ and corresponding to residues methionine 25 for $^{his}T_G$, serine 23 for $^{his}U_H$, arginine 22 for $^{his}W_J$, and arginine 23 for $^{his}X_K$ relative to the prepiline peptidase cleavage site were generated following the strategy used for $XcpT_G$ and $XcpX_K$ described in Ref. 18, where $XcpT_{G\text{-}NH}$ and $XcpX_{K\text{-}NH}$ are now called $^{his}T_G$ and $^{his}X_K$, respectively. Briefly, plasmids pET-$^{his}U_H$ and pET-$^{his}W_J$ were generated as follows. The genes encoding pseudopilin-soluble domains were PCR-amplified using primers 5′UpC1 (BamHI;His_6) and 3′UpC2 (HindIII) for *xcpU*$_H$ and 5′WpC1 (BamHI;His_6) and 3′WpC2 (HindIII) for *xcpW*$_J$. The PCR introduced a region encoding an N-terminal His_6 tag together with BamHI/HindIII cloning sites. PCR products were first subcloned into the pCR2.1 vector (Invitrogen) and sequenced. BamHI/HindIII DNA fragments were then generated and subcloned into pET22b (Novagen). The cloning created an in-frame fusion of the *xcp* genes with the *pelB* region encoding the N-terminal signal sequence and under the control of the T7 promoter of the pET22b. In this way the recombinant protein could be produced in the periplasm. Production of the recombinant proteins was performed in the *E. coli* BL21 (DE3) strain (Invitrogen) grown in ZYP-5052 auto-inducing medium. After 4 days of growth, His_6-tagged pseudopilins were purified from the periplasmic fraction by affinity chromatography following the procedure previously described in (18) with an additional step of gel filtration on HiLoad 16/60 Superdex 75 (Pharmacia) in buffer: 50 mM sodium phosphate, 150 mM NaCl, pH 7. The purified proteins were concentrated using Centricon (Millipore) with a cut-off size of 5 kDa. The final sample concentrations were 13.1 mg/ml for $^{his}T_G$, 2.2 mg/ml for $^{his}U_H$, 4.4 mg/ml for $^{his}W_J$, and 1.4 mg/ml for $^{his}X_K$ as evaluated by the Bradford colorimetric test.

Affinity Measurements—Steady state or kinetic analysis of the interaction between different pseudopilins was performed on BIAcore 1000 at 25 °C. All of the buffers were 0.2-μm filtered and degassed before use. We indicate with ΔRU the variation of the resonance plasmon signal recorder upon addition of a ligand to the surface of the chip or addition of an analyte to the previously immobilized protein. The CM5 (carboxymethylated dextran) sensor chip was coated with V_I and X_K (pI > 8), immobilized by amine coupling (ΔRU = 300–700). The immobilization of the other Xcp was prevented by their low pI. A control flow cell was activated for amine coupling and desactivated, under conditions identical to the other flow cells. Solutions of X_K, T_G, U_H, W_J, V_I, the binary mix W_J-X_K, and the ternary mix, W_J-X_K-U_H (0.625–30 μM in 50 mM phosphate, pH 7.0, 150 mM NaCl, 0,005% surfactant P20) were passed over the flow cell with V_I and X_K covalently bound and on the control flow cell. Binding traces were recorded for three to six concentrations of analyte, in duplicate. In each cycle, 50 μl of buffer (50 mM phosphate, pH 7.2, 150 mM NaCl, 0,005% surfactant P20) were injected first to stabilize the base line; the analyte (80–320 μl) was then injected. No binding regeneration cycle was necessary because spontaneous dissociation was observed in each binding experiment.

The chip nickel-nitrilotriacetic acid was saturated with Ni^{2+} and regenerated with EDTA 350 mM. The buffer was 10 mM HEPES, pH 7.4, 150 mM NaCl, 0.005% surfactant P-20, supplemented with 0.05 mM EDTA for the continuous flow pump and 3 mM EDTA for the sample pump. The chip was first saturated with Ni^{2+} by washing it with 0.5 mM $NiCl_2$ (20 μl at 20 μl/min); one of the His_6-tagged pseudopilins ($^{his}U_H$, $^{his}W_J$, or $^{his}X_K$) was then passed over the chip (10–50 nM, 40 μl at 20 μl/min, ΔRU = 200–400), followed by the non-His_6-tagged pseudopilins (U_H, T_G, W_J, X_K, and V_I) (0.3125–5 μM in 10 mM HEPES, pH 7.4, 150 mM NaCl, 0,005% surfactant P20, 0.05 mM EDTA). In control traces, $NiCl_2$ injection was followed by injection of buffer (same volume as the His_6-tagged protein) and by the injection of the untagged proteins. The binding traces were recorded for three to six concentrations of analyte, in duplicate. Regeneration was achieved by washing the flow cell with 350 mM EDTA (20 μl at 20 μl/min). We were able to immobilize and get a stable signal for each of the His_6-tagged pseudopilin; nevertheless, in all cases but $^{his}U_H$, the very intense aspecific signal prevented a correct calculation of the interaction sensorgrams.

The chip streptavidine was used in 50 mM phosphate buffer, 150 mM NaCl, pH 7. Washing with 1 M NaCl and 50 mM NaOH was carried out as specified by the supplier before fixing biotinylated T_G and W_J (100 nM, 2–70 μl at 10 μl/min) at 500–600 ΔRU. Nonbiotinylated T_G, U_H, V_I, W_J, and X_K in 50 mM phosphate, 150 mM NaCl, pH 7, were passed over the flow cells (0.625–10 μM, 60 μl at 20 μl/min). The binding traces were recorded for four to five concentrations of analyte, in duplicate. No regeneration was necessary because spontaneous dissociation was observed. Reproducible interactions were detected only on immobilized W_J.

The aspecific signal for the experiments reported in supplemental Fig. S1 was 2–6% of the specific for V_I on X_K, X_K on V_I, and U_H on W_J, and 30–40% of the specific for W_J on V_I, W_J on U_H, and V_I on W_J. The aspecific signal for the experiments reported in Fig. 2 was 20–30% for W_J-X_K on V_I, and 7% for W_J-X_K-U_H on V_I. Aspecific binding was subtracted from binding traces before calculation. Dissociation constants (K_{diss}) can

be estimated with the BIA-Evaluation software either as the ratio of the kinetic dissociation and association constants (k_{off}/k_{on}) or on the basis of the steady state levels of ΔRU, directly related to the concentration of complex. Fitting of a secondary plot of the concentration of complex at different concentrations of analyte allows the estimation of K_{diss}. In the present case, k_{on} and k_{off} were always very fast, and their estimation has been possible only for the complex W_J-X_K. Indeed, as specified by the supplier in the case of BIAcore 1000, good estimations of k_{on} and k_{off} can be calculated for the values in the range 10^3–10^6 M^{-1} s^{-1} and 10^{-5}–10^{-2} s^{-1}, respectively. Out of these ranges, the error of the estimation is very large.

T_G and W_J have been biotinylated with Sulfo-NHS-SS-Biotin (Pierce) following the protocol specified by the supplier, with minor modifications. The proteins were diluted at 25 μM in 50 mM phosphate buffer, 150 mM NaCl, pH 7.5, and the reactive was added at 100 μM (molar ratio, 4:1). The reaction was let going for 4 h on ice. To eliminate the excess reactive, the protein solutions were first filtered on NAP-5 column (GE Healthcare) equilibrated in the same buffer as specified above and then dialyzed by NOVAGEN Dialyzer Midi (cut-off, 3.5 kDa) against two times 400 ml of the same buffer as specified above at 4 °C overnight.

Batch Co-purification of Pseudopilin Soluble Domains—We used as bait His_6-tagged pseudopilin soluble domains. All of the experiments were carried out at 4 °C. In reaction mixture 1 (RM1), ^{his}N (where "N" designates any pseudopilins) was incubated in 1 ml of equilibration buffer (50 mM Tris-HCl, pH 8, 300 mM NaCl, 10 mM imidazole) with 200 μl of 5% nickel-nitrilotriacetic acid magnetic bead solution (Qiagen) pre-equilibrated in equilibration buffer. In reaction mixture 2 (RM2), the untagged pseudopilin partners were incubated in 1 ml of equilibration buffer. Both RM1 and RM2 were placed on a rotary shaker and gently mixed for 1 h. RM1 was placed on a magnet for 1 min to catch the magnetic beads. The flow-through was discarded, and the magnetic beads were rinsed twice with 500 μl of equilibration buffer including for each wash 1 min of mixing on the rotary shaker and 1 min of catch on the magnet. Then RM2 was mixed with the ^{his}N-coated magnetic beads issued from RM1 and gently mixed on the rotary shaker for 1 h. After 1 min catch on the magnet, the flow-through was discarded, and the magnetic beads were washed with 500 μl of wash buffer (50 mM Tris-HCl, pH8, 300 mM NaCl, 20 mM imidazole) six times, including for each wash 1 min of mixing on the rotary shaker and 1 min of catch on the magnet. Proteins specifically bound to the magnetic beads were then eluted with 100 μl of elution buffer (50 mM Tris-HCl, pH 8, 300 mM NaCl, 500 mM imidazole) two times, including for each elution 1 min of mixing on the rotary shaker, a spin at 8734 × *g* to pellet the beads, and 1 min of catch on the magnet. To analyze each fraction, 18 μl of protein samples were mixed with 6 μl of 4× concentrated SDS loading buffer. The 24-μl samples were boiled for 10 min and then loaded and run on a 15% SDS-PAGE gel as described in Ref. 18. After electrophoresis, the gels were stained with Coomassie Blue. For each co-purification experiment, the following amount of pseudopilins has been used: $^{his}T_G$ (137 μg), $^{his}U_H$ (71 μg), $^{his}W_J$ (259 μg), T_G (116 μg), U_H (95 μg), V_I (49 μg), W_J (150 μg), and X_K (119 μg).

Quantification of Bands from Polyacrylamide Gels—Coomassie Blue-stained gels were scanned. The digitalized gels were then analyzed with the free software "ImageJ for Mac" (24) to quantify and compare the intensity of the protein bands.

Native-PAGE and Two-dimensional SDS-PAGE—The eluted complex presented in Fig. 3*C* (*panel 1*, *lane E*) has been electrophoresed on a Native 8–16% Tris-HCl PAGE (Bio-Rad) at 4 °C in a Tris/Glycine running buffer for 1 h at 50 V and a further 2 h at 125 V. The native-PAGE was then stained with Coomassie Brillant Blue R-250. The entire lane containing the electrophoresed pseudopilin complexes was then cut off the gel, wrapped in plastic film, and boiled in a water bath for 30 min for complex dissociation. The lane was inserted horizontally into the large well of a 15% SDS-PAGE, together with purified proteins in other wells. After electrophoresis under denaturing conditions, the gel was stained with Coomassie Brillant Blue R-250.

RESULTS

Systematic Analysis for Interactions between the Five Xcp Pseudopilin-soluble Domains—We have analyzed the interaction between the five Xcp pseudopilin soluble domains of *P. aeruginosa* T2SS by using surface plasmon resonance (BIAcore). Three types of immobilization were used: covalent amine coupling to the chip CM5, affinity binding to the chips nickel-nitrilotriacetic acid, and streptavidine. For all of the interactions tested, the K_{diss} values were found in the micromolar range, and for all interactions but one (see below), the association and dissociation rate (k_{on} and k_{off}) were too fast to be calculated, suggesting a transient association. The estimation of the K_{diss} values was carried out by plotting the ΔRU value at steady state level, directly related to the concentration of complex, as a function of the concentration of analyte.

First, we investigated systematic binary interaction between pseudopilins; primary surface plasmon resonance data are presented in supplemental Fig. S1. Each immobilized pseudopilin has been exposed to all of the other pseudopilins, including itself. The interaction between two given pseudopilins has been detected twice, with one or the other partner immobilized (Fig. 1 and supplemental Fig. S1). In all of the cases but one (discussed below), the calculated K_{diss} values are slightly different (two to four times) but in the same order of magnitude.

Binding results were recorded in the presence of immobilized U_H, V_I, W_J, and X_K, whereas immobilized T_G did not show any significant binding (supplemental Fig. S1). The histidine-tagged U_H ($^{his}U_H$) was found to interact only with W_J. The calculated K_{diss} value is 0.72 or 2.85 μM, depending whether $^{his}U_H$ or W_J was immobilized (Fig. 1 and supplemental Fig. S1). V_I interacts with W_J and X_K. The K_{diss} for the couple V_I-W_J is 4.6 or 1.6 μM when V_I or W_J is immobilized, respectively. The K_{diss} value for the couple V_I-X_K is 19.8 and 1.55 μM when V_I or X_K is immobilized, respectively. The significant discrepancy in K_{diss} value (~10-fold difference) observed with the couple V_I-X_K might be ascribed to a partial hindrance of the binding site of V_I, the smallest partner, when immobilized. It should be noted that the orientation of the protein immobilized on chip

A

BOUND LIGAND	ANALYTE: T_G (12kDa)	U_H (16kDa)	V_I (11kDa)	W_J (24kDa)	X_K (34kDa)
T_G (SA)	-	-	-	-	-
$^{his}U_H$ (NTA)	-	-	-	**0.72±0.12**	-
V_I (CM5)	-	-	-	**4.6±0.2**	**19.8±0.4**
W_J (SA)	-	**2.85±0.15**	**1.6±0.2**	-	-
X_K (CM5)	-	-	**1.55±0.85**	-	-

B

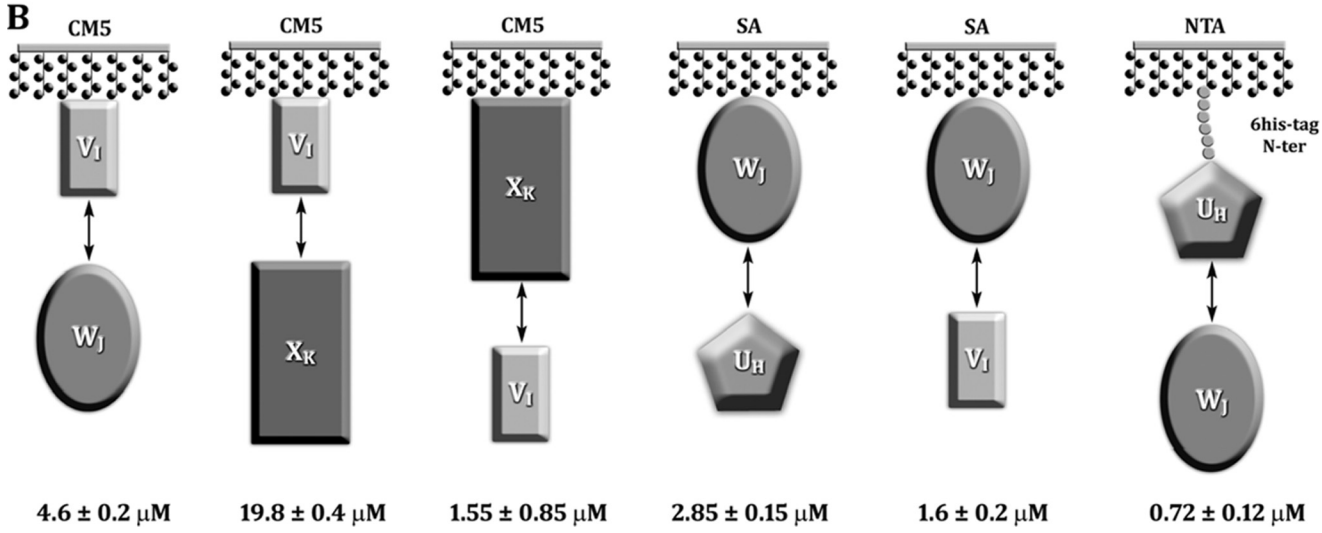

FIGURE 1. **Pseudopilin interaction network using surface plasmon resonance (BIAcore).** *A*, each ligand was tested with the five analytes. The K_{diss} values (μM) for the interaction were detected. In parentheses are the chip used for each ligand and the molecular mass of each analyte. *B*, schemes for all positive interactions, with the K_{diss} values indicated.

CM5 by amine coupling and on chip streptavidine by the interaction streptavidine-biotine is random, because it depends on the distribution of lysines on the protein surface. Moreover, the immobilization itself may reduce the protein mobility and accessibility compared with a protein freely diffusing in solution. As a result, restricted interaction at the binding site may occur with a bigger probability when the immobilized protein is small.

It is important to note that T_G interacts neither with itself nor with any other pseudopilins and that none of the pseudopilins forms homodimers. Moreover, it is tempting and may not be worthless to make a relation between the transitory nature of all the interactions detected, between domains of the pseudopilins, and the ephemeral existence frequently proposed for the type II pseudopilus.

Our systematic approach clearly identified three interactions U_H-W_J, V_I-W_J, and V_I-X_K. We further investigated whether the two partners of a single pseudopilin bind at the same or at two different sites.

Epitope Mapping and Binary and Ternary Interaction of Xcp Pseudopilin-soluble Domains—To determine the position of the binding sites and further elaborate on the pseudopilin complex organization, we exposed V_I to several analytes (Fig. 2): W_J first, followed by a mix of W_J-X_K and W_J-X_K-U_H.

At a concentration of 5 μM, the binding of W_J-X_K mix to V_I is characterized by a larger amplitude compared with the binding of W_J and X_K alone on V_I (Fig. 2, *A* and *B*) and a slower and therefore measurable k_{on} (3×10^3 M^{-1} s^{-1}) and k_{off} (7×10^{-3} s^{-1}); the affinity of the W_J-X_K mix (3 μM) is slightly higher but close to that of W_J alone (4.6 μM) and much higher than for X_K alone (19.8 μM) (Fig. 1). The change in amplitude and binding pattern compared with the one of W_J and X_K alone validate the formation of a complex between V_I, W_J, and X_K. Because we did not find any binary interaction between W_J and X_K independently, we propose that W_J and X_K both bind V_I, but at distinct epitopes (Fig. 2*C*).

To further investigate the interaction network between the pseudopilin soluble domains, we studied the binding of W_J-X_K-U_H ternary mix on V_I covalently bound and compared the

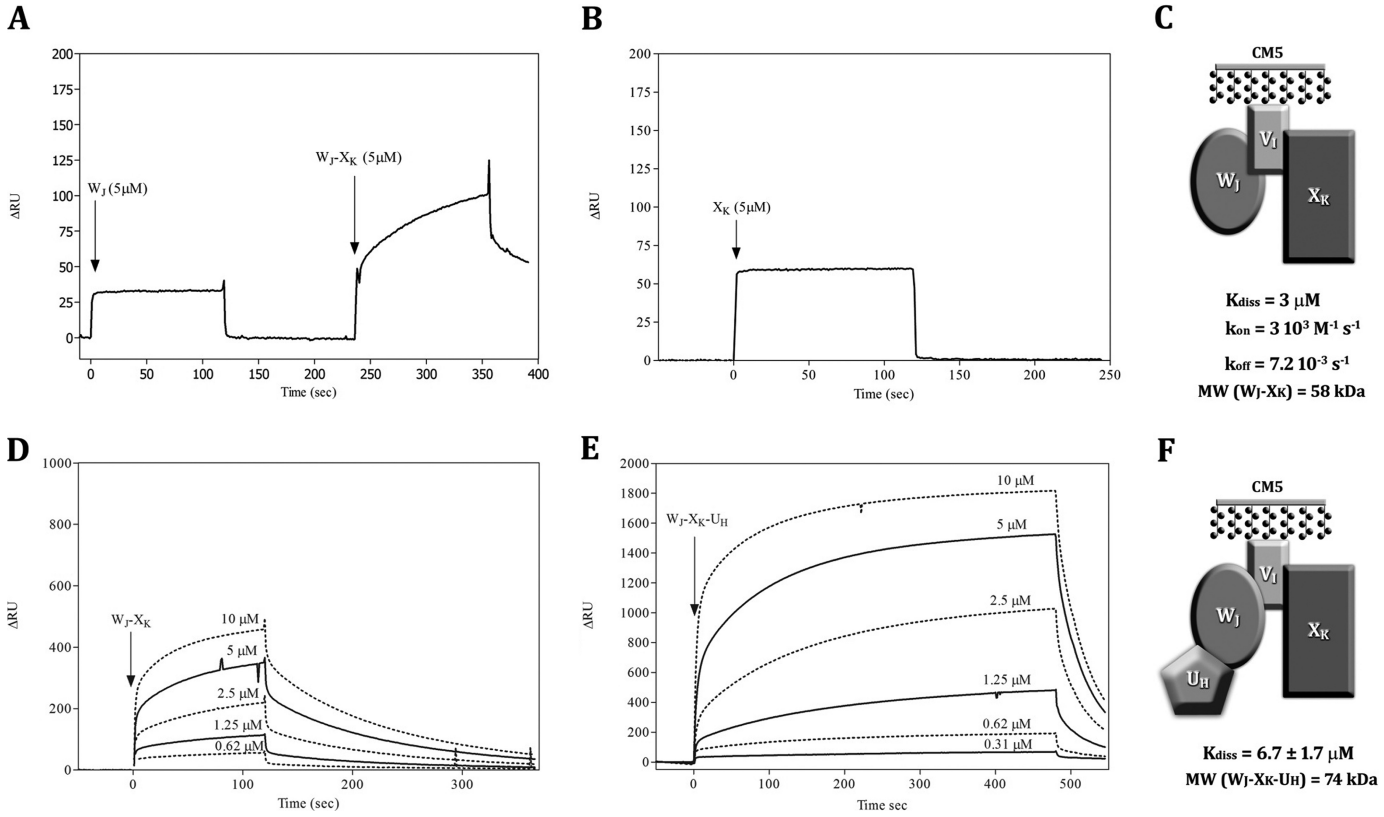

FIGURE 2. **Epitope mapping and binary and ternary interaction of pseudopilin soluble domains using surface plasmon resonance (BIAcore).** *A*, W_J (5 μM) and binary mix W_J-X_K, (5 μM) were passed on V_I bound to a CM5 chip. *B*, binding pattern of X_K alone (20–1.25 μM) on V_I bound to a CM5 chip. *D*, binding pattern of binary mix W_J-X_K (10–0.62 μM) on V_I bound to a CM5 chip. *E*, binding pattern of W_J-X_K-U_H mix (10–0.31 μM) on V_I bound to a CM5 chip. *A*, *B*, *D*, and *E*, we report on the *y* axis the variation of plasmon resonance in arbitrary unit (ΔRU) and the reaction time on *x* axis. *C* and *F*, schemes of the W_J-V_I-X_K and U_H-W_J-V_I-X_K complexes proposed, with K_{diss} of the interaction and k_{on} and k_{off} values when calculable.

results with those found for the W_J-X_K mix on V_I. The purpose of this study is to demonstrate the possible influence of a third component on the binding on V_I. The ternary mix W_J-X_K-U_H binds to V_I and presents a K_{diss} value of 6.7 μM, two times larger than that of W_J-X_K (3 μM); the amplitude also is four to five times larger than that of W_J-X_K (Fig. 2, *D* and *E*). The change in amplitude and binding pattern with the ternary mix compared with the one obtained with binary mixes suggests the formation of a quaternary complex. As previously proposed, the epitopes of W_J and X_K on V_I are distinct (Fig. 2*C*), and U_H only binds W_J (Fig. 1). We therefore propose the existence of a quaternary complex where V_I plays a central role with X_K and W_J, on which U_H binds (Fig. 2*F*).

Characterization of the XcpU$_H$-W$_J$-V$_I$-X$_K$ Pseudopilin Quaternary Complex—To thoroughly provide evidence for the assembly of the quaternary pseudopilin complex suggested by BIAcore experiment, we performed affinity co-purification between all the pseudopilin soluble domains. For these experiments we used both tagged (^{his}N) and untagged (N) pseudopilins. By affinity co-purification (see "Experimental Procedures"), $^{his}W_J$ was able to pull-down U_H (Fig. 3*A*, *panel 1*, *lane E*) in a specific manner because U_H could not bind to the magnetic beads in the absence of $^{his}W_J$ (Fig. 3*A*, *panel 2*, *lane E*), thus confirming the U_H-W_J interaction. Then X_K and V_I were both co-purified with $^{his}W_J$ (Fig. 3*B*, *panel 1*, *lane E*), confirming the existence of a ternary complex between V_I, W_J, and X_K (Fig. 3*B*, *panel 1*). Because X_K could not be co-purified with $^{his}W_J$ in the absence of V_I (Fig. 3*B*, *panel 2*, *lane E*), we confirm by this approach that V_I is the linker connecting W_J to X_K in the ternary complex formed by W_J, V_I, and X_K pseudopilin-soluble domains. This observation validates that W_J and X_K do not interact directly and form a ternary complex via V_I.

Interestingly, U_H added as a fourth partner in the affinity purification assay was co-purified together with the ternary complex $^{his}W_J$-V_I-X_K (Fig. 3*C*, *panel 1*, *lane E*), confirming the identification of the quaternary complex U_H-V_I-W_J-X_K. The integrity of the quaternary complex seems to rely on the presence of V_I because the absence of V_I triggered a massive loss of X_K co-purification with $^{his}W_J$ (Fig. 3*C*, *panel 2*, *lane E*). We showed that the small amount of X_K eluted in the absence of V_I (Fig. 3*C*, *panel 2*, *lane E*) is not bound to $^{his}W_J$ and corresponds to the nonspecific binding of X_K to the column because at least an equal amount is eluted in the absence of $^{his}W_J$ (supplemental Fig. S2, *C* and *D*). We then concluded that X_K associates to the complex through V_I. In contrast, we observed that U_H remains significantly bound to $^{his}W_J$ in absence of V_I (Fig. 3*C*, *panel 2*), which is in agreement with a direct interaction between U_H and $^{his}W_J$ (Fig. 3*A*, *panel 1*). Quantification of the bands corresponding to U_H and X_K in Fig. 3*C* (*panels 1* and *2*) shows that, after subtracting the nonspecific binding for both proteins, X_K is completely lost in the absence of V_I, whereas one-fourth of U_H is still significantly associated to $^{his}W_J$ (supplemental Fig. S2). Thus, U_H can still bind to $^{his}W_J$ in the absence of V_I and X_K, albeit with a decreased affinity, assuming that the affinity of U_H

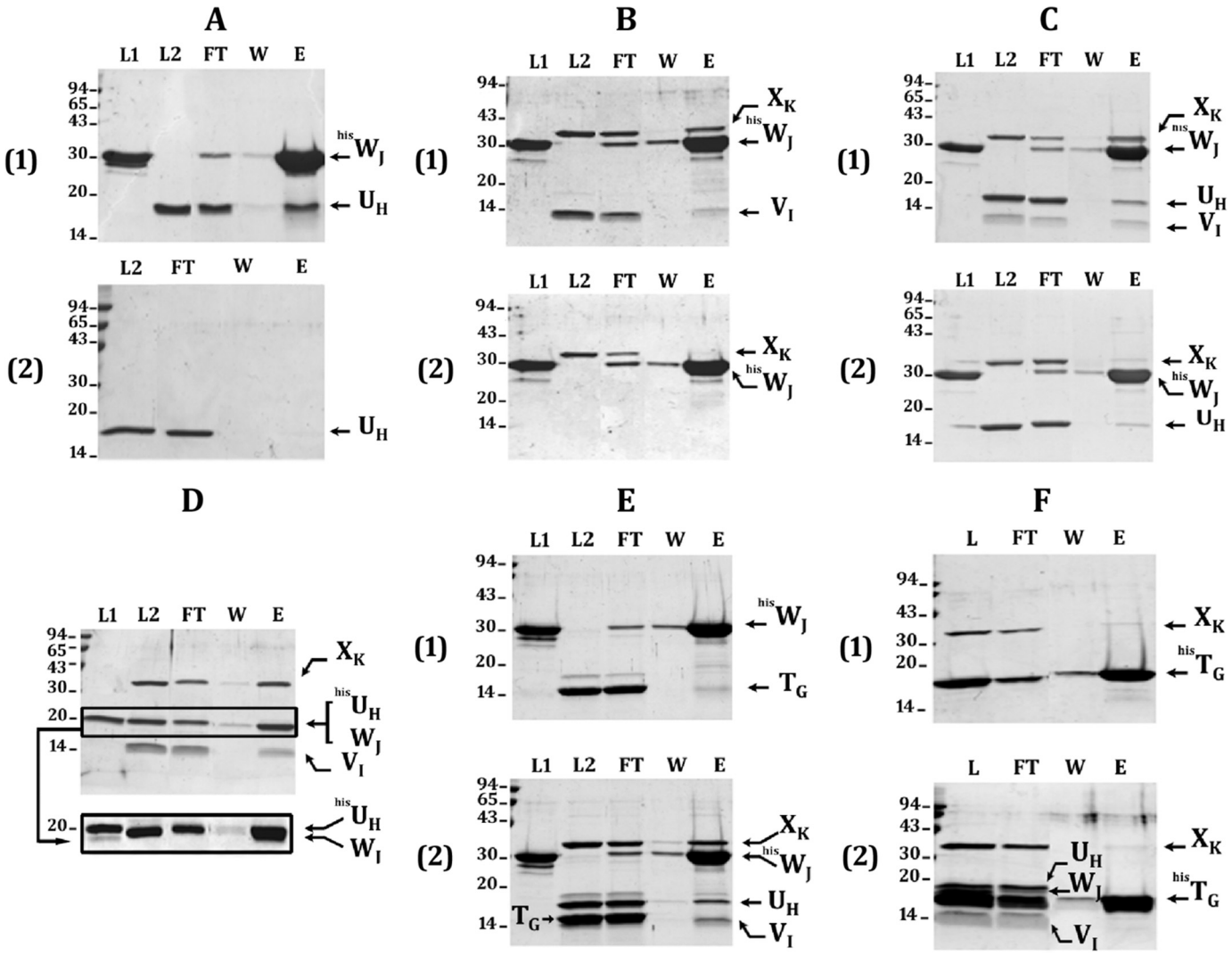

FIGURE 3. **Batch co-purification of pseudopilin-soluble domains on affinity column.** Each of the His_6-tagged protein was mixed with different untagged protein partners to dissect the pseudopilin quaternary complex. W_J-U_H interaction is shown in *A*; the requirements of V_I for the formation of W_J-V_I-X_K ternary and U_H-W_J-V_I-X_K quaternary complexes are presented in *B* and *C*, respectively; *E* and *F* demonstrate that T_G does not integrate the U_H-W_J-V_I-X_K quaternary complex. After affinity co-purification of proteins bound to the Ni^{2+}-NTA-magnetic beads, the collected fractions were analyzed on a 15% SDS-PAGE. After electrophoresis, the gel was stained with Coomassie Blue. *Fractions L1*, *L2*, and *L*, respectively, contain the His_6-tagged protein, the untagged protein partners, or both tagged and untagged proteins. *Fraction FT* contains the flow-through, *fraction W* contains the final wash, and *fraction E* contains the eluate. The positions of molecular mass markers are indicated on the *left side* of each gel (kDa). The positions of the various pseudopilin periplasmic domains are indicated on the *right side* of each gel or lane. In *D*, when the samples were run on a 12% SDS-PAGE for a longer time, the $^{his}U_H$ and W_J bands could be distinguished (surrounded with a frame), but under these conditions, V_I runs out of the gel (not shown). The presence of $^{his}U_H$ and W_J in the doublet band (*lane E*) was confirmed by mass spectrometry. The *faint band* present just below $^{His}W_J$ in the presence or not of other pseudopilins corresponds to a $^{His}W_J$ degradation product, as confirmed by mass spectrometry analysis.

is improved by the presence of V_I and X_K. We are therefore tempted to propose that the W_J-V_I-X_K trimeric complex could be a prerequisite for the proper integration of U_H into the complex. Finally, the comparison between the two co-purification experiments in the presence or absence of U_H (Fig. 3, compare panels 2 in *B* and *C*) shows that X_K does not interact with W_J even in presence of U_H, a result that confirms the central role for V_I in the initiation of the quaternary complex.

To further confirm the formation of the U_H-W_J-V_I-X_K quaternary complex, we tested the co-purification of $^{his}U_H$ together with the three other minor pseudopilin-soluble domain (Fig. 3*D*). The experiment showed that $^{his}U_H$ could co-purify V_I, W_J, and X_K (Fig. 3*D*), confirming the formation of the quaternary complex.

Moreover, we clearly show that the soluble domain of XcpT could not integrate the quaternary complex formed by the minor pseudopilin-soluble domains. We first tested the co-purification of $^{his}W_J$ together with T_G in presence or absence of the three other minor pseudopilins. The results presented in Fig. 3*E* indicate that T_G could not bind $^{his}W_J$ even in presence of V_I, U_H, and X_K. In addition, when using $^{his}T_G$ as bait, none of the minor pseudopilins could be co-purified (Fig. 3*F*). Altogether, the data presented in Fig. 3 (*E* and *F*) indicate that the T_G-soluble domain does not interact with any component of the minor pseudopilin quaternary complex either alone or in complex.

Direct Evidence of the Existence of the Quaternary Complex $Xcp^{his}W_J$-U_H-V_I-X_K—Using affinity co-purification we have clearly shown that the periplasmic domains of the four minor

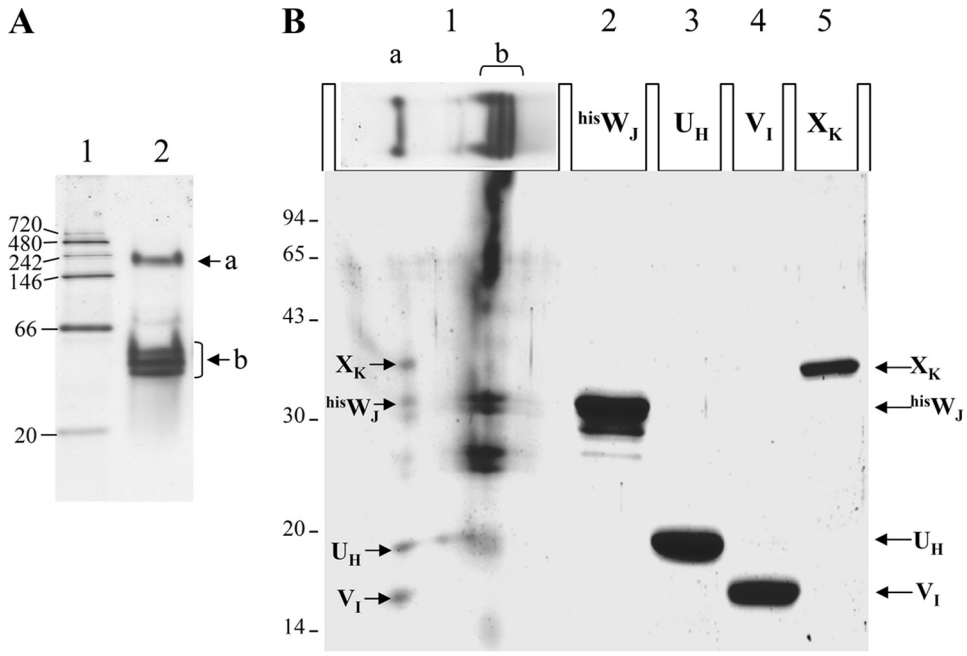

FIGURE 4. **Direct evidence of the quaternary complex Xcp $^{his}W_J$-U_H-V_I-X_K.** *A*, native 8–16% Tris-HCl PAGE (Bio-Rad) showing the migration of a native low molecular mass marker (*lane 1*) and the quaternary complex eluted from the co-purification presented in Fig. 3*C* (*panel 1*, *lane E*). The position of the two major, "a" and "b" native complexes are indicated. *B*, second dimension: 15% SDS-PAGE showing the composition of the complex isolated from the Native-PAGE. *Lane 1* contains the entire *lane 2* from *A* that has been cut off, boiled, and placed horizontally in the slot (see "Experimental Procedures"). *Lanes 2-5* contain purified hisW$_J$, U$_H$, V$_I$, and X$_K$, respectively. The positions of the pseudopilins periplasmic domains are indicated on the *right* and reveal the presence of four of them in the quaternary complex (*a*) and of Xcp^{his}W$_J$and XcpU$_H$ in the binary complex (*b*). Denaturated low molecular mass markers are shown on the *left* of the gel.

Xcp pseudopilins interact together, which proves indirectly the existence of the quaternary complex W_J-U_H-V_I-X_K. To show the physical existence of this quaternary complex, we have subjected the previously eluted complex (Fig. 3*C*, *panel 1*, *lane E*) to native-PAGE. The migration of the eluted quaternary complex on the native-PAGE is presented in Fig. 4*A* (*lane 2*). Interestingly, the complex dissociates in two major bands, a upper band (Fig. 4*A*, *a*) migrating right below the 242-kDa native marker and a lower band (Fig. 4*A*, *b*) migrating below the 66-kDa native marker. To analyze the composition of the two bands, the entire *lane 2* of the native PAGE has been cut off, boiled, and run on a SDS-PAGE (see "Experimental Procedures"). The results, presented in Fig. 4*B*, show that the upper band (*a*) is composed of the four minor pseudopilins, thus revealing their association in a quaternary complex, whereas the lower band (*b*) is composed of the already identified $^{his}W_J/U_H$ pseudopilin binary complex (Fig. 3*A*, *lane E*). We think that the lower band is composed of the excess of the tagged protein ($^{his}W_J$), and the upper band is probably the true stoichiometric quaternary complex.

DISCUSSION

By using a combination of protein-protein interaction approaches, we have investigated the interaction network between the soluble domains of the five pseudopilins involved in the *P. aeruginosa* T2SS. The T2SS piston model previously proposed (25) suggests that the secretion process requires the assembly of a pseudopilus, which pushes the exoprotein out of the cell and through the OM secretin.

The present work together with pseudopilin three-dimensional structures (12, 14, 15, 17) confirm that two distinct complexes contribute to the pseudopilus structure. First, the pseudopilus core is formed by the homomultimerization of the major pseudopilin through interaction between hydrophobic domains. Second, an heteromeric complex contains at least three of the minor pseudopilins (17). During the pseudopilus biogenesis, the assembly of these complementary structures can follow two possible scenarios. In the first, the pseudopilus core forms first, and the minor pilin complex integrates the pseudopilus from its base, thus stopping its elongation. Alternatively, the minor pilin complex forms first, and underneath takes place the assembly of the pseudopilus core. As a result the minor pseudopilin complex will be located at the tip and elongation may stop because of interaction with the OM secretin. Several arguments are in favor of the presence of the minor pseudopilin complex at the tip of the pseudopilus: 1) the requirement of XcpV$_I$ to initiate pseudopilus formation (18); 2) the interaction between XcpW$_J$ and the secretin (20); and 3) the recent publication of the structure of a ternary complex formed by the three pseudopilins GspI$_V$-J$_W$-K$_X$, which has been proposed to be at the tip of the pilus because no pseudopilin could be added upward (17).

In our study, it is important to recall that we used the soluble domains of the pseudopilins to investigate the interaction network. Under those conditions all of the interactions involving the hydrophobic domain are lost, and likely all interactions involving the formation of the core pseudopilus will not be identified by our approach. The observation that the soluble domain of the major pseudopilin of the pseudopilus core, XcpT$_G$, does not interact with any of the other pseudopilins including itself confirmed this assessment.

However, we could show that XcpV$_I$, W$_J$, and X$_K$ do interact and form a ternary complex as previously reported (17). It is worth noting that our BIAcore and co-purification data clearly showed that XcpW$_J$ and XcpX$_K$ do not interact directly but are bridged by XcpV$_I$, on which they bind at distinct sites. This observation further puts forward XcpV$_I$ as a nucleator in the formation of the pseudopilin complex and the subsequent formation of the pseudopilus. This central initiating role of XcpV$_I$ is also in agreement with previous findings indicating that XcpV$_I$ is the only pseudopilin required for the formation of the XcpT$_G$ HPP (9, 18).

An additional new feature that we revealed with our work is that the tip complex might be formed by the four minor pseu-

dopilins. Indeed we clearly demonstrated that $XcpU_H$ does interact directly with $XcpW_J$ and with $XcpW_J$ only. Significantly, this interaction seems to be more efficient when $XcpW_J$ is already bound onto the V_I-X_K complex. If this is the case, it means that $XcpU_H$ is the last minor pseudopilin to enter the complex and is thus likely to be located at its base.

If $XcpU_H$ is located at the base of the minor pseudopilins complex, it makes sense to suggest that $XcpU_H$ could form the hinge between the tip complex and the core pseudopilus formed by $XcpT_G$. Moreover, concerning the connection between the $XcpT_G$ core pseudopilus and the $XcpV_I$-W_J-X_K tip complex, several additional arguments are favoring a linker position for $XcpU_H$: 1) As indicated, Yanez et *al.* (14) solved the tridimensional structure of the $GspH_U$-soluble domain and suggest by docking experiments to place it at the tip of the $GspG_T$ pseudopilus with its specific conserved crevice facing away from the helix axis; whether $GspH_U$-specific crevice is involved or not in the interaction with $GspJ_W$ remains an open question. 2) Kuo *et al.* (19) have shown a direct interaction between full-length $GspH_U$ and $GspG_T$ pseudopilins.

It is worth noting that we were not able to show an interaction between soluble domains of $XcpU_H$ and $XcpT_G$, which suggests that if an interaction exists, as suggested above, it should be through the hydrophobic domain. Again this is very much in favor of the idea that once $XcpU_H$ integrates the minor pseudopilins complex, it will allow the further elongation of the pseudopilus core by integrating the $XcpT_G$ pseudopilin via its hydrophobic segment.

In the literature many more interactions have been found between pseudopilins (19, 21), and it would be extremely difficult to reconcile in a realistic model all of these observations, such as the formation of homo- or heterodimers between basically all of these pseudopilins. However, among all the interactions reported, it cannot be excluded that some involve rather unspecific contacts between the hydrophobic domains. *In vivo*, the hydrophobic interaction network may be regulated by the proximity of the soluble domains avoiding the addition of subsequent pseudopilins by steric hindrance. From this point of view, the characterization of the interaction network between soluble domains has revealed a relevant and specific network in which only some interactions are allowed, revealing thus the sequence of assembly necessary to obtain an appropriate configuration of the quaternary complex at the tip of the pseudopilus. Because we showed that the $XcpT_G$-soluble domain displays no interaction with other pseudopilin soluble domains, we propose that it may enter the structure through its hydrophobic domain. Once integrated, it will fit best with the addition of subsequent $XcpT_G$ pseudopilins, which will result in pseudopilus growth.

$XcpT_G$ may also access the minor pseudopilin complex through interaction with the hydrophobic domain of a pseudopilin other than $XcpU_H$. In that case the stability of the scaffold may not be optimal, and the pseudopilus growth might be aborted because of instability and collapse of the whole structure. It was for example suggested that direct interaction between $XcpX_K$ and $XcpT_G$ resulted in $XcpT_G$ instability (18). If this was the case, the formation of the tip complex could be a prerequisite for the assembly of a proper pseudopilus structure,

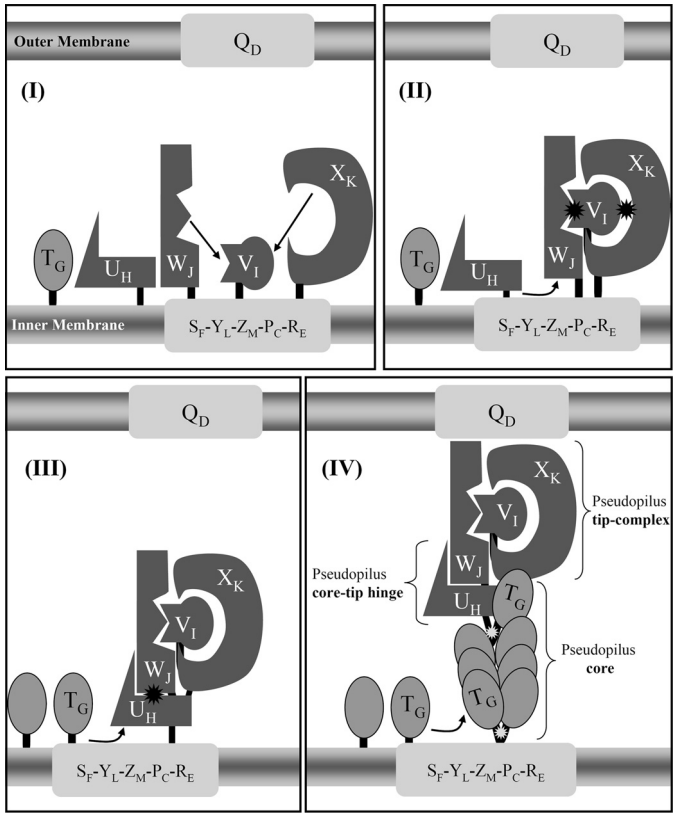

FIGURE 5. **Interaction network among Xcp pseudopilins and model for pseudopilus assembly.** A schematic representation of the Xcp T2SS of *P. aeruginosa* is proposed. The inner membrane plate form, composed of $XcpS_F$, -Y_L, -Z_M, -P_C, and -R_E and the outer membrane secretin $XcpQ_D$ are shown as *light gray rectangles*. The minor pseudopilins, $XcpU_H$, -V_I, -W_J, and -X_K are represented by differently shaped forms (*dark gray*) that illustrate the complementarity of their interaction interfaces. For instance, $XcpV_I$ can interact with both $XcpW_J$ and $XcpX_K$, with two different interaction sites. The *black asterisk* indicates that the interaction involves the periplasmic domains of the pseudopilins. The major pseudopilin $XcpT_G$ is shown as an oval shape (*medium gray*) that can interact with itself during pseudopilus assembly, as well as with $XcpU_H$. The *white asterisk* indicates that these interactions involve the transmembrane domains of the pseudopilins. We proposed the following ordered series of events leading to the assembly of the pseudopilus: *Panel I*, $XcpV_I$ enters first the inner membrane plateform and then recruits both $XcpW_J$ and $XcpX_K$ to form the pseudopilus tip complex. *Panel II*, $XcpU_H$ then enters the ternary complex $XcpV_I$-W_J-X_K via its interaction with $XcpW_J$. *Panel III*, the tip quaternary complex is then able to accommodate the major pseudopilin $XcpT_G$ via a "hydrophobic" interaction with $XcpU_H$. *Panel IV*, further polymerization of $XcpT_G$ pseudopilins triggers pseudopilus growth, with $XcpU_H$ fulfilling a core-tip hinge function between the pseudopilus core and tip.

which retains its functionality to propel protein secretion. This fine tuning in pseudopilus assembly may, however, be overruled when the stoichiometry is totally unbalanced by the massive overproduction of $XcpT_G$, which results in HPP assembly. However, it is worth noting that the HPP structure is then totally unable to support protein secretion appropriately.

In conclusion and as presented in Fig. 5, we propose that XcpV is the central component and initiator of pseudopilus formation. Although it does not directly interact with the $XcpT_G$ core component, it is central to the ordered assembly of a complex, which will be located at the tip of pseudopilus. The assembly of the complex is sequentially monitored by interactions between their soluble domains, which give high specificity and do not allow alternative sequence in the assembly process of a quaternary complex (heterotetramer). Once the complex is

formed, the last component that is integrated, $XcpU_H$, will allow its hydrophobic domain to interact with the $XcpT_G$ hydrophobic domain. Subsequent interaction could only result in pseudopilus growth through $XcpT_G$ multimerization. The elongation of the pseudopilus might be arrested by contact of the tip complex with the secretin. At this level, the extrusion of the pseudopilus is prevented by the bulky domain of $XcpX_K$, which does not fit the interior of the secretin channel. This arrest may in turn induce retraction of the pseudopilus. If exoproteins are found to locate between the tip complex and the secretin, events of elongation/retraction should result in shots of exoprotein release through the secretin channel, according to the T2SS piston model earlier proposed (25).

Future work is necessary to explore the validity of the pseudopilus model. Protein-protein interaction studies and structural resolution of the different components have provided crucial data in developing further our understanding of this fascinating system. Now that the question on elongation seems to lead to a consensus agreement, the questions around the retraction aspects should be addressed further. In particular, we will address the suggested role of $XcpX_K$ in that process by evaluating the role of its soluble domain both in protein secretion and HPP formation.

Acknowledgments—We are grateful to Hervé Darbon for constant help and support, to Christophe Quetard for useful suggestions on BIAcore experiments, and to Renaud Vincentelli for help in cloning and expression of pseudopilin-soluble domains. We thank Sabrina Lignon and Régine Lebrun from the Plate-forme Protéomique de l'Institut de Microbiologie de la Méditerranée, Marseille Protéomique, CNRS (Marseille, France) for matrix-assisted laser desorption ionization time-of-flight mass spectrometry analyses.

REFERENCES

1. Pugsley, A. P. (1993) *Microbiol. Rev.* **57,** 50–108
2. Voulhoux, R., Ball, G., Ize, B., Vasil, M. L., Lazdunski, A., Wu, L. F., and Filloux, A. (2001) *EMBO. J.* **20,** 6735–6741
3. Filloux, A. (2004) *Biochim. Biophys. Acta*. **1694,** 163–179
4. Pelicic, V. (2008) *Mol. Microbiol.* **68,** 827–837
5. Craig, L., and Li, J. (2008) *Curr. Opin. Struct. Biol.* **18,** 267–277
6. Bally, M., Filloux, A., Akrim, M., Ball, G., Lazdunski, A., and Tommassen, J. (1992) *Mol. Microbiol.* **6,** 1121–1131
7. Bleves, S., Voulhoux, R., Michel, G., Lazdunski, A., Tommassen, J., and Filloux, A. (1998) *Mol. Microbiol.* **27,** 31–40
8. Nunn, D. N., and Lory, S. (1993) *J. Bacteriol.* **175,** 4375–4382
9. Vignon, G., Köhler, R., Larquet, E., Giroux, S., Prévost, M. C., Roux, P., and Pugsley, A. P. (2003) *J. Bacteriol.* **185,** 3416–3428
10. Durand, E., Bernadac, A., Ball, G., Lazdunski, A., Sturgis, J. N., and Filloux, A. (2003) *J. Bacteriol.* **185,** 2749–2758
11. Hu, N. T., Leu, W. M., Lee, M. S., Chen, A., Chen, S. C., Song, Y. L., and Chen, L. Y. (2002) *Biochem. J.* **365,** 205–211
12. Köhler, R., Schäfer, K., Müller, S., Vignon, G., Diederichs, K., Philippsen, A., Ringler, P., Pugsley, A. P., Engel, A., and Welte, W. (2004) *Mol. Microbiol.* **54,** 647–664
13. Hansen, J. K., and Forest, K. T. (2006) *J. Mol. Microbiol. Biotechnol.* **11,** 192–207
14. Yanez, M. E., Korotkov, K. V., Abendroth, J., and Hol, W. G. (2008) *J. Mol. Biol.* **377,** 91–103
15. Yanez, M. E., Korotkov, K. V., Abendroth, J., and Hol, W. G. (2008) *J. Mol. Biol.* **375,** 471–486
16. Lam, A. Y., Pardon, E., Korotkov, K. V., Hol, W. G., and Steyaert, J. (2009) *J. Struct. Biol.* **166,** 8–15
17. Korotkov, K. V., and Hol, W. G. (2008) *Nat. Struct. Mol. Biol.* **15,** 462–468
18. Durand, E., Michel, G., Voulhoux, R., Kürner, J., Bernadac, A., and Filloux, A. (2005) *J. Biol. Chem.* **280,** 31378–31389
19. Kuo, W. W., Kuo, H. W., Cheng, C. C., Lai, H. L., and Chen, L. Y. (2005) *J. Biomed. Sci*. **12,** 587–599
20. Douet, V., Loiseau, L., Barras, F., and Py, B. (2004) *Res. Microbiol.* **155,** 71–75
21. Lu, H. M., Motley, S. T., and Lory, S. (1997) *Mol. Microbiol.* **25,** 247–259
22. Bogomolovas, J., Simon, B., Sattler, M., and Stier, G. (2009) *Protein Expr. Purif.* **64,** 16–23
23. Veesler, D., Blangy, S., Siponen, M., Vincentelli, R., Cambillau, C., and Sciara, G. (2009) *Anal. Biochem.* **388,** 115–121
24. Abramoff, M. D., Magelhaes, P. J., and Ram, S. J. (2004) *Biophotonics Int.* **11,** 39–42
25. Filloux, A., Michel, G., and Bally, M. (1998) *FEMS. Microbiol. Rev.* **22,** 177–198